Macromolecules

pubs.acs.org/Macromolecules Article

Anisotropic Coarse-Grained Model for Conjugated Polymers: Investigations into Solution Morphologies

Alexander E. Cohen, Nicholas E. Jackson,* and Juan J. de Pablo*

Cite This: *Macromolecules* 2021, 54, 3780−3789 Read Online

ACCESS | Metrics & More | Article Recommendations | Supporting Information

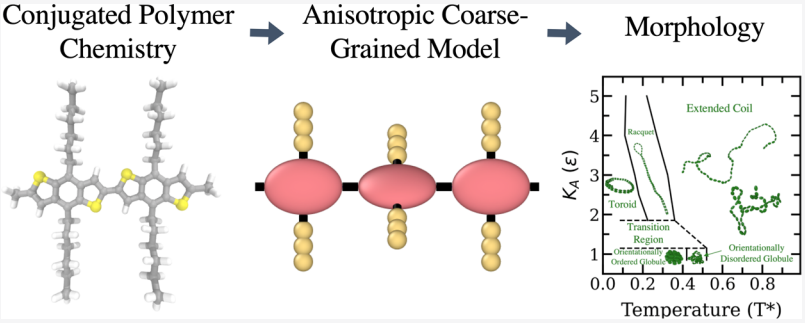

ABSTRACT: The optoelectronic properties of conjugated polymers are dictated by the interplay of multiscale structural features, including intrachain dihedrals, interchain $\pi-\pi$ stacking, and the complex mesoscale morphology. While much is known about the structures of polymers with isotropically interacting monomers, little is known about polymers with strongly anisotropic backbone monomers, a class of materials to which conjugated polymers belong. Fundamental understanding is further complicated when the semiflexible and molecularly heterogeneous nature of conjugated polymers is taken into account. We present an anisotropic coarse-grained (CG) model for conjugated polymers that incorporates key molecular features (monomer anisotropy, intermonomer dihedrals, and side chains). The model is employed to characterize the single-chain conformational properties of conjugated polymers, revealing a rich temperature-dependent conformational landscape. These studies provide a critical link between CG molecular descriptors and conformational ordering in conjugated polymers.

INTRODUCTION

Conjugated polymers are organic materials that combine the mechanical and thermophysical properties of synthetic polymers with the optoelectronic properties of inorganic semiconductors. The semiconducting nature of conjugated polymers, which facilitates visible light absorption, charge generation, and electronic conductivity, arises from the sp^2 hybridization of carbon atoms along the polymer backbone. Conjugated polymers also maintain many of the desirable attributes of nonconjugated polymers, including tunable molecular weights and processing protocols that can enable mechanical flexibility,[1] optical transparency,[2] and roll-to-roll processing.[3−5] Combinations of these properties are favorable for a variety of applications in optoelectronic devices, including photovoltaics (PVs),[6−9] thin-film transistors,[10−13] light-emitting diodes,[14−16] and biosensors.[17,18]

To engineer conjugated polymers, it is critical to understand the nuclear degrees of freedom that dictate optoelectronic functions. It is well known that intramolecular charge and exciton transport along conjugated polymer chains are controlled by the relative dihedral angles of monomers along the conjugated backbone.[19−21] If neighboring monomers are coplanar, the overlap of neighboring carbon 2p-orbitals is maximized and transport of electrons is efficient; if neighboring monomers are oriented perpendicularly, p-orbital overlap is reduced[22] and charges become trapped. Similarly, intermolecular charge and exciton transport are dictated by the overlap of p-orbitals of monomers on different chains via $\pi-\pi$ stacking.[23] At mesoscopic length scales, the ability of transport pathways to percolate a bulk film[24,25] will be controlled by larger length scale features such as polymer crystallinity, grain boundaries, and tie chains[26−28] which are set by overall chain size, persistence lengths, and nematic ordering of the full polymer chain. To holistically describe both molecular and mesoscopic features that dictate functions in conjugated polymers, accurate multiscale models that consider molecular and mesoscopic structures on equal footings are key to advancing materials design.

Received: February 8, 2021
Revised: March 15, 2021
Published: April 7, 2021

https://doi.org/10.1021/acs.macromol.1c00302
Macromolecules 2021, 54, 3780−3789

Throughout the past 4 decades, researchers have devised numerous design strategies for engineering the optoelectronic properties of conjugated polymers via molecular modifications. Many of these design rules have focused on the engineering of conjugated monomers and the use of copolymerizations for targeted changes in valence band, conduction band, and optical gap energy levels.[29,30] While critically important, this emphasis on the molecular electronic structure does not capture the vital element of material morphology that is well known to control soft materials functionality. To this end, experiments have made progress by focusing on the roles that solubilizing side chains, $\pi-\pi$ stacking, solution aggregation, and rational processing protocols play in controlling the mesoscale ordering of conjugated polymers.[27,31−37] These studies have confirmed that mesoscopic ordering has a significant impact on optoelectronic properties, and it is apparent that understanding this mesoscopic ordering is key to controlling performance in conjugated polymers. Particularly, one must understand how molecular design rules at the monomer scale, when combined with processing conditions, manifest in the mesoscopic polymer structure. The complexity of this task has made the navigation of the design space for conjugated polymers challenging and costly to access experimentally. To this end, multiscale theory and computation are particularly well poised to help experimental efforts navigate through this complex design space.

In contrast to quantum-chemical and atomistic molecular dynamics (MD) simulations of conjugated polymers, coarse-grained (CG) and mesoscopic modeling for these materials have been relatively rare.[38−53] One reason for this relative scarcity in CG design principles involves the nature of the intermolecular interactions that dictate structure formation in conjugated polymers. Conjugated monomers often contain fused aromatic rings with strongly anisotropic intermolecular interactions, leading to the disk-like stacking of conjugated monomers known as $\pi-\pi$ stacking. Moreover, these fused aromatic rings come in a variety of synthetically accessible shapes, sizes, interaction strengths, and flexibilities. When these details are combined with flexible and diverse side-chain architectures, variable solvents, and molecular additives, attributing morphological features to the specific molecular structure becomes extremely challenging. As a final compounding factor, simulation timescales capable of accessing equilibrium or pseudo-equilibrium morphologies are usually unreachable by fully atomistic simulations. In traditional polymer physics, searching this vast molecular design space is aided by the use of simple but powerful CG models, such as the isotropically interacting bead-spring and Kremer−Grest models[54,55] that have been pivotal in exploring the effects of various polymer architectures, molecular weights, and processing protocols on mesoscopic structural properties. The assumption of isotropic interbead interactions is common for CG models as isotropic interactions are straightforward to implement and exhibit a low computational cost. Since most CG computational tools rely on isotropic interactions, whereas the critical degrees of freedom which dictate structure formation in conjugated materials are inherently anisotropic, it is hardly surprising that the field lacks a strong understanding of how CG molecular descriptors manifest in the resulting conjugated polymer morphologies. It is reasonable to hypothesize that if a CG model could be developed that includes anisotropic monomers coupled to intermonomer dihedrals, the powerful CG computational protocols that have been so successful for nonconjugated polymers could be translated to conjugated polymers.

In this paper, we introduce a CG model specific to conjugated polymers that captures the critical molecular degrees of freedom unique to conjugated polymers (anisotropic monomer interactions, intermonomer dihedrals, and semiflexibility) while simultaneously being computationally efficient and capable of exploring mesoscopic length scales. First, we introduce the CG model and describe its parameters, making specific connections to experimentally or quantum-chemically derived quantities. We then incorporate this new model into a parallel tempering protocol that enables efficient sampling of single-chain conjugated polymer conformations at a range of temperatures and use this scheme to explore strategic modifications in the molecular structure of conjugated polymers. The results of these simulations reveal a rich diversity of conformational states for conjugated polymers accessible by tuning the fundamental molecular parameters of the CG model. We believe that this model provides an efficient tool for sampling the conformational space of conjugated polymers while incorporating the critical degrees of freedom common to the vast space of monomer chemistries and thus should be useful for future morphology design efforts for conjugated polymers.

METHODS

Model Description. In what follows, we develop a CG model that captures three critical degrees of freedom necessary for describing conjugated polymers: (i) anisotropically interacting monomers linked by intermonomer dihedral potentials, (ii) polymer semiflexibility, and (iii) isotropically interacting side-chain chemistries. The philosophy of our CG model involves representing conjugated polymers using a mixture of isotropic Lennard-Jones (LJ) and anisotropic CG potentials, similar to seminal early works modeling liquid crystals.[49,56] In this mixed representation, independent fused conjugated rings are represented by anisotropic CG particles,[39,41] whereas nonconjugated portions of the polymer are represented using isotropic CG particles. A key feature of our model involves the addition of dihedral potentials between nearest-neighbor anisotropic monomers; given the critically important role of intermonomer dihedrals for controlling intrachain electronic transport, which would be entirely absent in standard isotropic CG models, these terms are included explicitly in our CG model.

For maximum flexibility in the intermolecular potentials of anisotropic particles, we utilize the biaxial Gay−Berne (GB) equation for dissimilar particles[57] using the formalism of Everaers and Ejtehadi[58] as implemented in LAMMPS.[59] Due to the cumbersome form of the equations to describe this potential energy surface, we provide a brief description of the key parameters here and encourage readers to explore the original work for a thorough description. The GB potential computes an anisotropic LJ interaction between pairs of dissimilar ellipsoidal/spherical particles according to the expressions of eqs 1−3

$$U(\mathbf{A}_1, \mathbf{A}_2, \mathbf{r}_{12}) = U_r(\mathbf{A}_1, \mathbf{A}_2, \mathbf{r}_{12}, \gamma)\cdot\eta_{12}(\mathrm{A}_1, \mathrm{A}_2, \nu)\cdot \chi_{12}(\mathbf{A}_1, \mathbf{A}_2, \mathbf{r}_{12}, \mu) \quad (1)$$

$$U_r = 4\varepsilon(\rho^{12} - \rho^6) \quad (2)$$

$$\rho = \frac{\sigma}{h_{12} + \gamma\sigma} \quad (3)$$

$$\varepsilon_a = \sigma\cdot\frac{a}{b\cdot c} \quad (4)$$

$$\varepsilon_b = \sigma\cdot\frac{b}{a\cdot c} \quad (5)$$

https://doi.org/10.1021/acs.macromol.1c00302
Macromolecules 2021, 54, 3780−3789

$$\varepsilon_c = \sigma \cdot \frac{c}{a \cdot b} \tag{6}$$

where a, b, and c control the shape of the ellipsoid in the side, face, and end-to-end dimensions, respectively, and γ and μ can be used to further customize the shape of the Gay−Berne interactions. In this work, γ and μ are both set to 1.0, and the values of the varying anisotropic well depths are set explicitly without reference to the shapes of the ellipsoids. All interaction parameters between dissimilar particles are mixed according to geometric mixing rules. A global interaction cutoff of 3.0 σ is used, and no shifts are applied due to the anisotropic nature of the potential. Cutoffs beyond 3.0 σ were tested but exhibited qualitatively similar results.

Reduced LJ units are used throughout the work, with ε and σ characterizing the energy and length scales of the system, respectively. For this work, ε (epsilon) is in units of the thermal energy at room temperature k_BT, and σ is set such that 1 $\sigma \approx 0.7$ nm, which is roughly equivalent to the diameter of a benzene ring. The GB potentials within the CG model are parameterized by ε_i and σ_i, which are expressed in terms of the characteristic ε and σ for the model. We direct readers to the original biaxial GB work for a thorough discussion of all intermolecular interaction parameters.[57] As our current study focuses only on equilibrium chain properties, the masses of all beads are set equal to 1. Dynamical properties of this model will be explored in a future work.

The extended π-electron system of conjugated polymers is known to induce semiflexibility along the polymer backbone, as characterized by a finite persistence length related to the decay of a bond vector correlation function. To incorporate local stiffness along the polymer backbone, harmonic two-body bond stretching potentials, harmonic three-body angle potentials, and OPLS-style four-body dihedral potentials[49,56] between anisotropic monomers have been included in the CG model (Figure 1). A key feature of the CG model is the use of noninteracting "ghost" atoms as off-center attachment sites for defining bonds and angle bends that allow for forces and torques to be applied to anisotropic monomers instead of simply acting on the center of mass (COM) (Figure 1B). In this work, off-center attachment sites exist between neighboring ellipsoids and adjacently bonded ellipsoids or bonded side-chain beads. This implies that side-chain free simulations exhibit two off-center bonding sites per ellipsoid positioned along the bond axis, and half dense side-chain simulations exhibit three off-center bonding sites, with one occurring 90° rotated within the π-system plane. Dense side-chain simulations exhibit four off-center bonding sites per ellipsoid. The model used in this work incorporates harmonic bonds and harmonic angles between a combination of COM positions and off-center attachment sites in order to represent both anisotropic monomers and side chains. However, the model is designed in such a way as to give the user maximum flexibility in bonding geometries through arbitrary combinations of COM and off-center bonding sites.

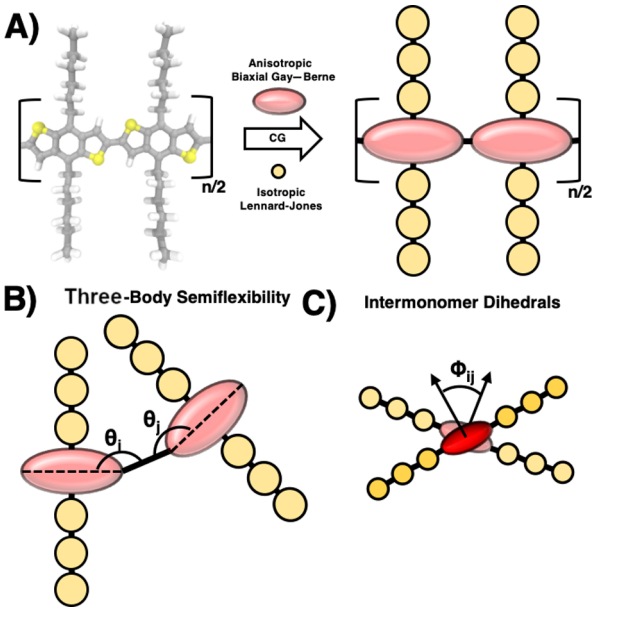

Figure 1. Schematic of the CG model for conjugated polymers. (a) CG mapping procedure, (b) three-body angle definition between anisotropic monomers using off-center attachment sites, and (c) dihedral angle definition between nearest-neighbor anisotropic monomers (looking down the polymer bond axis).

The beads that participate in a single three-body angle definition are shown in Figure 1B. In isotropic CG models, it is common to implement backbone stiffness via the use of three-body angle potentials applied between neighboring monomer COMs. While this procedure would technically enforce the necessary backbone semiflexiblity in the CG model, it would not penalize the free rotations of the GB monomers and would consequently not be able to faithfully represent $\pi-\pi$ stacking. To address this point, harmonic bonds and angles between anisotropic monomers are implemented using rigid off-center attachment sites that restrict free rotation while enforcing chain semiflexibility. A similar technique was used in the early modeling of liquid crystalline molecular dimers consisting of a combination of Gay−Berne and LJ beads.[49] The backbone semiflexibility resulting from the implemented three-body potential scheme is entirely equivalent to that induced by standard three-body potentials between COMs. This fact was confirmed by running simulations of CG chains using the off-center angle bend implementation, histogramming over the angles formed by neighboring monomer COM triplets, and Boltzmann inverting to obtain the effective three-body free-energy surfaces. These potentials were observed to be identical to those obtained by running a standard semiflexible chain simulation with three-body angle potentials applied between COMs and were further checked by comparison of persistence lengths to the values derived from a Kratky−Porod model (Figure S2B).

To enforce relative dihedral angles between neighboring anisotropic monomers that dictate electron delocalization along conjugated polymer backbones, we implement OPLS-style dihedral potentials between anisotropic monomers. This is accomplished using a scheme identical to our previous work which uses the orientation vectors of neighboring anisotropic monomers and the vector between neighboring COMs to compute the dihedral angle, from which forces are derived for MD.[41] This scheme is identical to standard implementations that integrate three-body and four-body potentials and fully decouples the dihedral degrees of freedom from the angular degrees of freedom. The dihedral implementation is validated against analytical results derived from the treatment of a linear chain of dihedrals by Rossi[60] and is shown in Figure S2A. For clarity, the equations governing all intramolecular potentials are provided in eqs 7−9. In the simulation results that follow, the three-body angle potential parameter, K_A, and the second harmonic coefficient in the OPLS cosine expansion, K_D, are used as the primary parameters for semiflexibility and dihedral barrier height, respectively,

$$E_{\text{bond}} = K_B(r - r_0)^2 \tag{7}$$

$$E_{\text{angle}} = K_A(\theta - \theta_0)^2 \tag{8}$$

$$E_{\text{dihedral}} = \frac{1}{2}K_1[1 + \cos(\phi)] + \frac{1}{2}K_D[1 - \cos(2\phi)] + \frac{1}{2}K_3[1 + \cos(3\phi)] + \frac{1}{2}K_4[1 - \cos(4\phi)] \tag{9}$$

Model Parameterization. As an exploratory simulation of the equilibrium properties of the CG conjugated polymer model, we selected phenomenologically motivated CG parameters consistent with a broad variety of conjugated polymer chemistries.

Degree of Polymerization. A value for the degree of polymerization was selected that is consistent with experimental conjugated copolymer syntheses. State-of-the-art conjugated materials

https://doi.org/10.1021/acs.macromol.1c00302
Macromolecules 2021, 54, 3780−3789

typically employ sizes that range between small oligomers[32] to a few hundred monomers.[61,62] For this work, a degree of polymerization of 64 (64 connected GB ellipsoidal monomers) was selected. This value is large enough to reduce large fluctuations in computed properties but small enough to limit the presence of entanglements that might hinder the approach to equilibrium.

Intermolecular Parameters. The simulations performed here utilize an implicit solvent representation in which the solvent has been incorporated via renormalized intermolecular interaction parameters and the use of a Langevin thermostat. This strategy is common in the field of soft materials,[63] although the model developed in this work is also amenable to particle-based explicit solvent representations. GB parameters of anisotropic monomers in this study were chosen to coarsely reflect a commonly used chemical architecture for optoelectronic applications[29] known as benzodithiophene (BDT) (Figure 1). The monomer has a diameter of approximately 7 Å along the bond axis, a 3 Å diameter along the $\pi-\pi$ stacking axis, and a 5 Å diameter along the perpendicular lamellar axis, as derived from a geometry optimization via the United Atom Force Field. These shape parameters are represented in the GB model by setting $\sigma_i = 1.0$, with relative well depths $\varepsilon_{i,a}$, $\varepsilon_{i,b}$, and $\varepsilon_{i,c}$ set to 1.0, 0.1, and 0.25, respectively (Figure S3). Provided the strongly aggregating and typically solvophobic nature of conjugated polymers even in a "good solvent",[64,65] a value of $\varepsilon_i = 1.0\varepsilon$ was selected for all performed simulations to avoid deep kinetic traps. While the nature of intermolecular parameter selection is phenomenological for this first exploration of the CG model, it is performed in the same spirit as standard Kremer–Grest-style CG models. Provided the significant literature on the use of Kremer–Grest models for implicit solvent simulations, we anticipate that for weakly anisotropic monomers, the position of the theta point should be similar to that of the isotropic model ($\varepsilon \approx 0.3$),[63] although clearly this will be violated for strongly anisotropic species, and constitutes a point of further investigation in the future. Simulations employing side-chain beads utilize the parameters $\varepsilon_{SC} = 0.01$ and $\sigma_{SC} = 0.25$.

Intramolecular Bonded Parameters. For equilibrium structural (not dynamical) properties, the specific values of two-body bond stretching parameters should have a minimal effect on model results. While many models employ the finite extensible nonlinear elastic (FENE) potential, the FENE potential is not formulated for bonds between anisotropic particles and thus is not used here. To enforce near rigidity in the two-body potentials, a value of $K_B = 200\ \varepsilon/\sigma^2$ is employed with $r_0 = 0.2\ \sigma$. This large value of K_B will limit the accessible time step but is a restriction that can be easily lifted in future work. All two-body stretching potentials for anisotropic/anisotropic, anisotropic/side chain, and side chain/side-chain beads also employ $K_B = 200\ \varepsilon/\sigma^2$ and $r_0 = 0.2\ \sigma$.

Three-body potentials are only applied between neighboring anisotropic beads to enforce semiflexibility. A range of three-body harmonic angle coefficients (K_A) are explored in this work that are consistent with the persistence lengths of conjugated polymers derived from small-angle neutron scattering experiments.[66] Values of K_A between 0 and 10 K_A/ε are used in this work, with $\theta_0 = 180°$.

OPLS dihedral coefficients between anisotropic monomers were determined by comparison to previous quantum-chemical calculations for conjugated polymers with the donor–acceptor motif.[67] From this study, the range of energy barriers between planar and perpendicular intermonomer orientations was determined to be 3–15 k_BT. For simplicity, we assume that only K_2 and K_4 affect the dihedral potential of the model. In what follows, "planar" backbones utilize $[K_1, K_2, K_3, K_4] = [0.0,K_D,0.0,0.0]$ and "nonplanar" backbones utilize $[K_1, K_2, K_3, K_4] = [0.0,0.0,0.0,-K_D]$.

Molecular Dynamics. MD simulations with a Langevin thermostat were employed to sample the equilibrium conformations of conjugated polymer chains using the developed anisotropic CG model. Langevin simulations used a damping parameter of 2 τ_{LJ}. A conservative time step of 0.00075 τ_{LJ} was used in conjunction with the large value of K_B for all final results, but larger time steps up to 0.01 τ_{LJ} are achievable, especially in the dilute and semidilute states. Single-chain simulations were performed using a parallel tempering scheme in order to overcome local kinetic traps and improve configurational sampling at all simulation temperatures. Previous work on molecular liquid crystals has successfully employed replica exchange schemes in the context of modified molecular Hamiltonians,[68] which constitutes a point of future investigation and development for the CG conjugated polymer model described here.

The parallel tempering proceeds as follows: first, a single-chain Langevin MD simulation is performed at a temperature of 1.5 until equilibrated chain conformations are obtained. Subsequently, uncorrelated chain configurations are selected from this trajectory and used to seed the starting configurations for the different replicas. Each replica is then annealed from the temperature of 1.5 to the target replica temperature over the course of 1,000,000 time steps. The temperature spacings between replicas are adjusted such that an acceptance ratio of 20–30% is achieved for all replicas.[69] Replica exchange swaps are generally very efficient above the coil-globule transition temperature but lose efficiency below this temperature (see Figure S4); future incorporation of more advanced sampling protocols is a natural augmentation of the current model. Trial replica swaps are performed every 100,000 time steps for a total simulation time of 100,000,000 time steps, or $7.5 \times 10^4\ \tau$, in each replica. For all reported results, eight statistically independent sets of simulations are performed utilizing distinct initial configurations and random number seeds in the velocity initialization and Langevin thermostats, the results of which are averaged to obtain the mean values reported in all figures. All CG model development and MD simulations are performed using the LAMMPS simulation package.[59]

RESULTS

Four distinct parameters sets of the CG model are employed to explore the effects of backbone planarity and side chains on the configurational space of conjugated polymers, as shown in Figure 2. Planar and nonplanar systems enforce potential

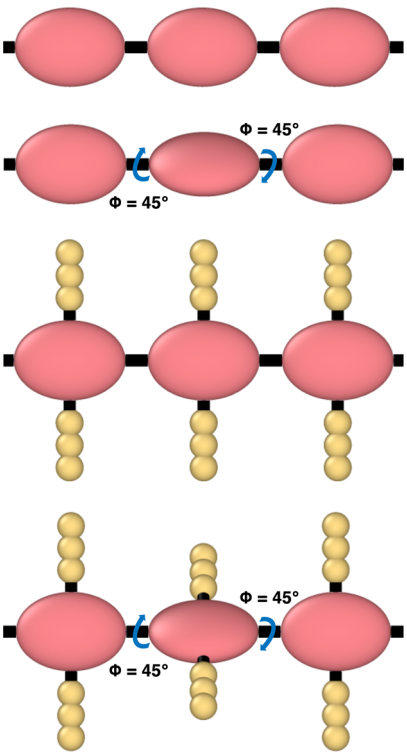

Figure 2. Four conjugated polymer architectures explored in this work. (A) Planar ($[0.0,K_D,0.0,0.0]$) without side chains, (B) nonplanar ($[0.0,0.0,0.0,-K_D]$) without side chains, (C) planar ($[0.0,K_D,0.0,0.0]$) with side chains, and (D) nonplanar ($[0.0,0.0,0.0,-K_D]$) with side chains.

https://doi.org/10.1021/acs.macromol.1c00302
Macromolecules 2021, 54, 3780–3789

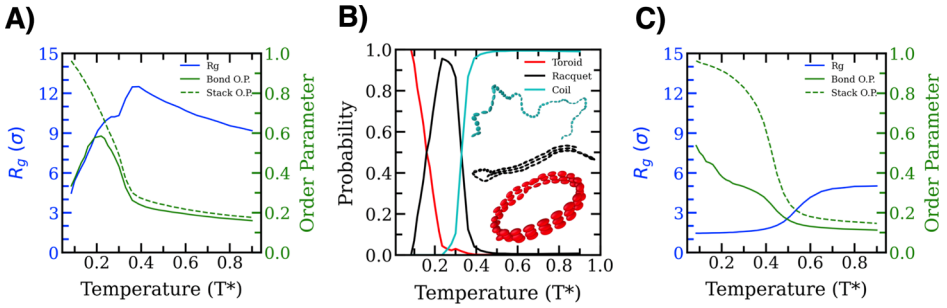

Figure 3. (a) Twin axis plot showing R_g and order parameters as a function of temperature for a planar dihedral polymer with no side chains (K_D = 3, K_A = 3). (b) Probability that the polymer (K_D = 3, K_A = 3) is in the coil, racquet, or toroid phases. (c) Twin axis plot showing R_g and order parameters as a function of temperature for a typical flexible polymer (K_D = 3, K_A = 1).

energy minima in the dihedral potential at 0/180 and 45/135°, respectively. In all cases, side chains use a three-CG-bead representation roughly consistent with the spatial dimensions of hexyl side chains that are ubiquitous in conjugated polymers.

Single-Chain Conformations without Side Chains. Provided the critical importance of solution-phase morphologies in dictating the neat-film structure in organic semiconducting applications,[35,70,71] we first explored the general behavior of dilute conjugated polymer conformations using the planar/no side-chain version of the CG model. To quantify conformational changes observed in simulations, we employed three metrics: the radius of gyration (R_g), a $\pi-\pi$ stacking order parameter ($S_{\pi-\pi}$), and a bond orientation order parameter (S_{bond}). The radius of gyration is computed in the standard fashion and monitors the coil-globule transition. $S_{\pi-\pi}$ and S_{bond} are derived from the largest eigenvalue of the Q-tensor[72] (eq 10) applied to all π-stacking vectors ($\hat{\mathbf{u}}_{\pi,i}$) perpendicular to the anisotropic monomers and nearest-neighbor anisotropic monomer bonding vectors ($\hat{\mathbf{u}}_{bond,i}$), respectively. $S_{\pi-\pi}$ reports on the average π-system orientation in the simulation, which is used to monitor the development of liquid-crystalline-like ordering within the conformations. S_{bond} reports on the average orientation of all bond vectors in the system and is useful for distinguishing between rod-like and coil/globule configurations

$$Q = \frac{1}{N}\sum_{i=1}^{N}\left(\frac{3}{2}\hat{\mathbf{u}}_{\pi/bond,i}\hat{\mathbf{u}}_{\pi/bond,i}^{T} - \frac{1}{2}I\right) \tag{10}$$

To complement the conformational characterizations of R_g, $S_{\pi-\pi}$, and S_{bond}, the radial distribution function (RDF) and directional RDF (d-RDF) were calculated to further characterize local orientational correlations within the system. To compute the d-RDF, we perform a standard RDF calculation except limited to a cone of arc length $\pi/8$ around the π-stacking vector orthogonal to the anisotropic GB monomers, with the normalization appropriately adjusted. The d-RDF reports on local π-stacking correlations and is helpful for differentiating over what length scales π-stacking persists within the aggregate.

Figure 3 displays the temperature dependence of conformations present in the planar CG model without side chains. Figure 3A shows the behavior of planar polymers without side chains (K_D = 3, K_A = 3) in which it is apparent that decreasing the temperature from 1.0 leads to an initial increase in R_g that is attributable to the polymer becoming more rod-like as the available thermal energy is lowered. At $T \approx 0.4$, a transition temperature is reached that is characterized by a decreasing R_g and strongly increasing $S_{\pi-\pi}$ and S_{bond} as T is lowered. This transition temperature is consistent with the transition from an extended coil-like structure to an aggregated structure with considerable intramolecular ordering. As the temperature is further lowered, R_g continues decreasing, $S_{\pi-\pi}$ continues to increase, and S_{bond} peaks. Visual analysis of trajectory snapshots combined with R_g and order parameter thresholding helps characterize the temperature dependence of the observed conformational states (Figure 3B), of which "coil", "racquet", and "toroid" are observed. The observed conformations as well as their associated temperature dependences are fully consistent with the temperature dependence of previous simulations of isotropic CG models of semiflexible polymer chains.[73−79] Specifically, it is observed that the extended coil and rod-like states are the stable high-temperature conformations. Upon a temperature decrease, collapse to a broad basin of metastable racquet conformations occurs, followed by a transition to toroidal conformations at the lowest temperatures. The peak in S_{bond} is due to the fact that the racquet phase has a larger value of S_{bond} than the toroid and coil phases. The reproduction of these conformations is strong evidence that the developed anisotropic CG model reproduces the fundamental conformational transitions well characterized by previous semiflexible models.

With the anisotropic CG model reproducing the known hierarchy of semiflexible conformational states, we next analyze the effect of the monomer anisotropy on the conformational states of the polymer. Specifically, in Figure 3C, the semiflexiblility of the chain is reduced to K_A = 1 (K_D = 3), and the temperature-dependent conformations are explored. In this case, we do not observe the conformational space associated with semiflexible polymers but instead observe the gradual coil-globule transition characteristic of flexible CG models. However, coincident with this gradual transition is the increase in ordering of the anisotropic monomers within the collapsed globule state. The results of Figure 3 constitute the critical general conformational features of the CG model, including the capability to reproduce the known temperature-dependent hierarchy of conformations for semiflexible polymers, combined with the use of anisotropic monomers capable of order in a "π-stacking" fashion, even in the relative absence of chain semiflexibility. This unified characterization of global semiflexible chain conformations and local molecular ordering is a critical feature of the developed model and is key to exploring future structure−function relationships in conjugated polymers.

We next systematically explore the CG model behavior as a function of both three-body semiflexibility (K_A) and dihedral

https://doi.org/10.1021/acs.macromol.1c00302
Macromolecules 2021, 54, 3780−3789

potential (K_D/K_4), examining both planar and nonplanar dihedrals. Figure 4A plots the temperature dependence of R_g

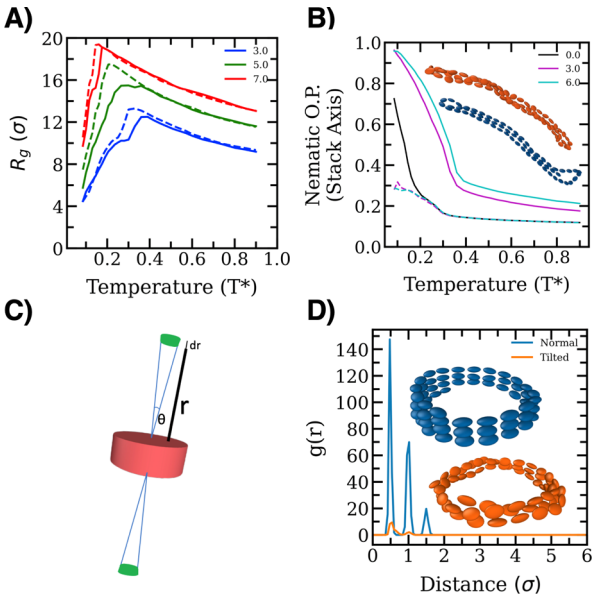

Figure 4. Comparison of planar and nonplanar dihedral CG models without side chains. (A) R_g as a function of temperature for semiflexible polymers with varying K_A and K_D or K_4 = 3.0. (B) $S_{\pi-\pi}$ as a function of temperature for semiflexible polymers with varying K_D, K_4, and K_A = 3.0. (C) Schematic of d-RDF. (D) d-RDF for toroid conformations with planar and nonplanar dihedrals (K_D or K_4 = 3, T = 0.085). For (A,B), solid lines are for polymers with planar dihedral minima; dotted lines are for polymers with dihedral minima at 45°.

for (i) planar/no side-chain and (ii) nonplanar/no side-chain polymers as a function of K_A. It is observed that as K_A increases, R_g increases at all temperatures, and the position of the coil-racquet transition shifts to lower temperatures, with no qualitatively new conformational features being observed. Nonplanar dihedrals exhibit larger R_g at lower temperatures than planar dihedrals, which is attributable to the inhibition of ordered anisotropic stacking, leading to an increase in the effective excluded volume of monomers in nonplanar chains relative to monomers in planar chains. Examination of MD snapshots combined with analysis of the d-RDF indicates that toroid formation at lower angle strengths results in smaller-diameter toroids with more π-stacking layers compared to toroids formed at higher angle strengths. Moreover, racquet phases at lower angle strengths are generally observed to exhibit more stacking layers and loops than the raquet phase at higher angle strengths, which is consistent with previous work.[76] Figure 4B shows $S_{\pi-\pi}$ for planar and nonplanar simulations as a function of the dihedral potentials K_D and K_4 (note: K_D = K_4 = 0 results in a chain with no constraints on dihedral degrees of freedom). As the dihedral barrier height (K_D) increases in planar polymers, the position of the onset of significant $S_{\pi-\pi}$ ordering shifts to higher temperatures, consistent with larger dihedral barriers being more robust to thermal disorder. However, for chains with nonplanar dihedral minima, increasing the dihedral barrier (K_4) strongly decreases the ability of the system to orientationally order. To further explore the low-temperature region, Figure 4C plots the d-RDF for the K_A = 3, K_D = 3 (planar)/K_4 = −3 (nonplanar) situations at T = 0.085, comparing planar and nonplanar dihedrals with equivalent barrier heights. While both systems form toroids at low temperature, it is clear that the nature of the local dihedral manifests strongly in the ability of the system to π-stack and consequently in the conformational properties of the toroids, with nonplanar dihedrals forming significantly less ordered toroids.

Single-Chain Conformations with Side Chains. Nearly all practically useful conjugated polymers employ molecular architectures with pendant, often alkylic side chains grafted to the main conjugated backbone (Figure 1A). To fully characterize the conformational space of conjugated polymers, it is thus vital to assess the role that solubilizing side chains play in dictating conformations. To begin exploring these effects within the context of the anisotropic CG model developed here, small chains of isotropic, purely repulsive side-chain particles were grafted from the backbone at two different densities: one side chain per anisotropic monomer and two side chains per anisotropic monomer. The side-chain architectures are shown in Figure 2 for the case of two side chains per anisotropic monomers—one side chain per anisotropic monomer consists of deleting one side chain from each anisotropic monomer, with the initial condition set up to be chain placement on alternating sides of the polymer axis.

In Figure 5A, we plot R_g as a function of temperature for three different side-chain densities for planar polymer back-

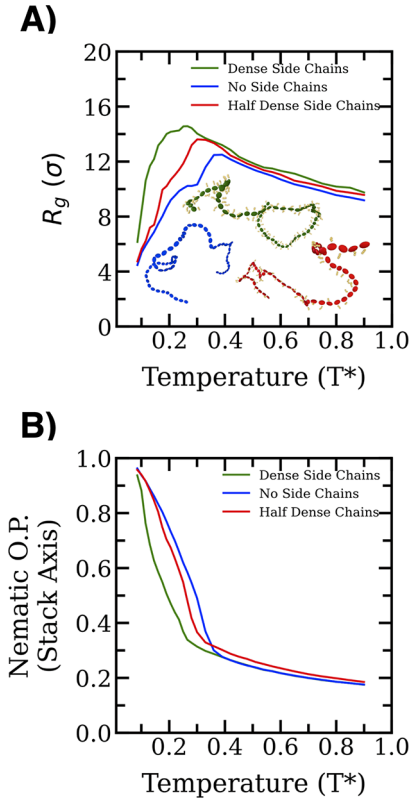

Figure 5. Conformational properties of the CG model with planar dihedrals (K_D = 3) and variable side-chain densities. (A) R_g and (B) $S_{\pi-\pi}$ as a function of temperature with varying side-chain densities.

bones. It is observed that the presence of side chains dramatically affects the observed conformational properties by shifting the position of the collapse transition to lower temperatures. A comparison to Figure 4A shows that the stiffening effect does not map cleanly onto an increase in the

https://doi.org/10.1021/acs.macromol.1c00302
Macromolecules 2021, 54, 3780−3789

effective semiflexibility of the backbone as its effect on conformations above the transition temperature is much weaker than that observed in Figure 4A. The effect manifests most strongly at low temperatures below the collapse transition, where side-chain interactions inhibit aggregation; this is likely the underlying conformational effect leading to improved solubility for conjugated polymers with side chains. Similar results were also realized for polymers with nonplanar dihedrals. The addition of side chains also impacts the $S_{\pi-\pi}$, as shown in 5B, with $S_{\pi-\pi}$ decreasing over all temperatures with increasing side-chain density, showing that side chains in the single-chain regime inhibit π-stacking order in the system. Also, analogous to how increased side-chain densities move the collapse transition to lower temperatures, increasing side-chain densities also moves the transition temperature for $\pi-\pi$ ordering to lower temperatures, consistent again with the ostensible use of side chains as solubilizers.

Conformational Design Space for Conjugated Polymers. Last, we examine the conformational space accessible to conjugated polymers with anisotropic monomers by plotting conformational phase diagrams as a function of K_A, which is the parameter observed to most strongly influence the conformational states formed for the CG model. Figure 6 summarizes the diversity of single-chain conformations available to semiflexible anisotropic polymers. For flexible anisotropic polymers, we observed two globule phases, one in which the dihedrals are well aligned and orientational ordering persists and one in which the dihedrals are not aligned that generally lacks orientational ordering. This orientationally disordered state exists at a higher temperature range than the orientationally ordered state, as would be anticipated. At high temperatures, we observed ideal chain and swollen chain polymer conformation states with the general understanding of single-chain polymer conformations. For semiflexible anisotropic polymers, we observed the known toroid, racquet, and rod-like coil phases that have been enumerated previously in the literature, including their appropriate relative temperature regimes. The transition regions between semiflexible and flexible polymers were not rigorously enumerated due to the difficulties of sampling these transition regions, although this certainly constitutes motivation for continuing work with this model.

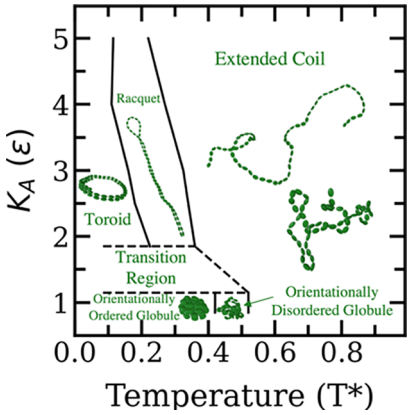

Figure 6. Qualitative phase diagram summarizing the space of obtainable conjugated polymer conformations as a function of temperature and chain semiflexibility. The results are obtained in the limit of planar dihedrals (K_D = 3.0) and no side chains.

DISCUSSION

The anisotropic CG model introduced in this work follows in the phenomenological spirit of other, highly successful isotropic CG models of the past 3 decades. The model implementation is validated for persistence lengths and dihedral correlation lengths via comparison to explicit analytical results of the Kratky−Porod model and the model of Rossi,[60] respectively. The model correctly reproduces the known relative stability of the coil/rod, racquet, and toroid states in the limit of large semiflexibility, while exhibiting additional molecular degrees of freedom associated with the anisotropy of monomers capable of incorporating π-stacking degrees of freedom. The CG model is useful in its ability to (i) simultaneously characterize both the large-length-scale conformational properties of semiflexible chains and short-length-scale anisotropic molecular degrees of freedom (intrachain dihedrals and $\pi-\pi$ stacking interactions) that define conjugated polymers and (ii) include the molecular heterogeneity and complexity characteristic of conjugated polymers (side chains and anisotropic shapes). This generalizability and flexibility, in combination with computational efficiency only marginally reduced compared to isotropic CG models, offers promise in a variety of important classes of prediction for conjugated materials, including PV, transistor, and bioelectronic applications.

One promising avenue for the anisotropic CG model proposed here is in the elucidation of the electronic properties of conjugated polymers at mesoscopic spatiotemporal scales, without the need for extensive backmapping and quantum-chemical procedures. Since the CG model preserves the critical spatial degrees of freedom required for describing π-electron overlap (intrachain dihedrals and relative π-stacking orientations), one can potentially incorporate electronic coarse-graining techniques[S1,S2] to enable electronic prediction entirely at the CG resolution, leading to a single resolution model capable of simultaneously characterizing the morphological and electronic structure of conjugated materials. While simultaneous morphological and electronic prediction has historically been obtained via a combination of isotropic CG models, atomistic backmapping, and repeat quantum-chemical calculations, the model described here has the potential to bypass these limitations and dramatically improve the scalability of design space predictions for conjugated materials. While the model has been developed at a lightly CG resolution here, there is the potential to incorporate the mixed isotropic/anisotropic bead description at larger length scales to further aid the exploration of mesoscopic length scales, similar to previous work.[46]

While the simulations in this work have been performed in the context of conjugated homopolymers, the anisotropic CG model presents opportunities for the interpretation of, and the direct application to, alternating donor−acceptor conjugated copolymers. Work by Kuei and Gomez[66] has obtained the experimentally and computationally derived persistence lengths of a broad variety of conjugated homopolymers and copolymers. While the anisotropic moiety in this work was loosely parametrized to represent a BDT unit, the results as a function of semiflexibility should be broadly applicable to any conjugated polymer chemistry, aiding in the interpretation of experimental characterizations in dilute conditions. Moreover, the anisotropic CG model itself can be easily adapted to incorporate arbitrary chemical complexity via the integration of

https://doi.org/10.1021/acs.macromol.1c00302
Macromolecules 2021, 54, 3780−3789

multiple, distinct anisotropic beads. The flexibility of the CG representation within our anisotropic CG model should expedite the modeling of conjugated polymer morphologies via the treatment of arbitrary fused-ring systems as anisotropic disks, enabling the mesoscale modeling of conjugated donor−acceptor polymers containing complicated fused-ring chemistries.

Moving forward, there are several directions for extension and improvement of the CG model outlined here. While it has been parameterized phenomenologically, an obvious improvement would involve the incorporation of rigorous coarse-graining protocols.[80−82] While the application of these rigorous CG techniques to anisotropic particles is generally limited, the additional anisotropic degrees of freedom maintained within the model can potentially improve model transferability[41] and thus constitute an important avenue of research moving forward. As anisotropic interactions are inherently suited to conjugated systems, this CG representation may be most suitable toward enabling these families of coarse-graining techniques for this materials class. There is also considerable potential for the use of advanced sampling techniques to help bypass the kinetically trapped states associated with strong intermolecular π-stacking interactions. In early liquid crystal work, this was implemented in the context of Hamiltonian replica exchange using soft anisotropic potentials,[68] and such a procedure would potentially be highly beneficial for the exploration of configuration space in dense packing.

CONCLUSIONS

We have developed an anisotropic CG model for exploring the conformational properties of conjugated polymers at mesoscopic spatiotemporal resolutions. The model employs a mixture of anisotropic and isotropic CG beads that capture the critical molecular degrees of freedom influencing conjugated polymer conformations and the electronic structure: anisotropic $\pi-\pi$ stacking, intermonomer dihedral angles, polymer chain semiflexibility. When integrated with a parallel tempering methodology, the CG model provides access to the conformational properties of single-chain conjugated polymers as a function of CG degrees of freedom. Specifically, we explore the influence of chain semiflexibility on the obtainable conformations in the solution phase. Simulations reproduced the hierarchy of polymer conformations known for semiflexible polymers (coil, racquet, and toroid) while also revealing conformational states unique to polymers with anisotropic monomers (e.g., the orientationally ordered globule). In all cases, $\pi-\pi$ stacking and dihedral ordering are quantified. The role of flexible side chains in mediating conjugated polymer conformations is also explored, with increasing side-chain density shifting the collapse transition temperature and the π-stacking ordering transition to lower temperatures. Finally, we provide a qualitative phase diagram as a function of chain semiflexibility that outlines the potential scope of polymer conformations anticipated for single chains of conjugated polymers. The CG model and results presented here present a solid foundation for developing a CG view of conjugated polymer physics akin to that developed for polymers with isotropic monomers over the past century.

ASSOCIATED CONTENT

Supporting Information

The Supporting Information is available free of charge at https://pubs.acs.org/doi/10.1021/acs.macromol.1c00302.

Validation of angle and dihedral potentials; persistence length and dihedral correlation length as a function of angle and dihedral potential coefficients (K_A,K_D) using CG MD simulations; comparison of dihedral correlation lengths calculated from simulation and theory (Rossi) in the limit of a rigid rod; comparison of persistence length calculated from simulation and theory (Kratky−Porod); intermolecular potentials; intermolecular potential energy surfaces for anisotropic monomer−anisotropic monomer pairwise interactions; replica exchange; and representative REMD sampling procedure showing the exchange of conformations between different temperature replicas (PDF)

AUTHOR INFORMATION

Corresponding Authors

Nicholas E. Jackson − *Department of Chemistry, University of Illinois, Urbana, Illinois 61801, United States;* orcid.org/0000-0002-1470-1903; Email: jacksonn@illinois.edu

Juan J. de Pablo − *Pritzker School of Molecular Engineering, University of Chicago, Chicago, Illinois 60637, United States; Center for Molecular Engineering, Argonne National Laboratory, Lemont, Illinois 60439, United States;* orcid.org/0000-0002-3526-516X; Email: depablo@uchicago.edu

Author

Alexander E. Cohen − *Pritzker School of Molecular Engineering, University of Chicago, Chicago, Illinois 60637, United States*

Complete contact information is available at: https://pubs.acs.org/10.1021/acs.macromol.1c00302

Notes

The authors declare no competing financial interest.

ACKNOWLEDGMENTS

This work was supported by the Department of Energy, Office of Science, Basic Energy Sciences, Materials Science and Engineering Division. The development of coarse-graining algorithms and software were supported by the Midwest Integrated Center for Computational Materials (MICCoM). We thank Dr. Alec Bowen, Dr. Phil Rauscher, and Dr. Liza Lee for helpful discussions.

REFERENCES

(1) Gustafsson, G.; Cao, Y.; Treacy, G. M.; Klavetter, F.; Colaneri, N.; Heeger, A. J. Flexible light-emitting diodes made from soluble conducting polymers. *Nature* **1992**, *357*, 477−479.

(2) Ugur, A.; Katmis, F.; Li, M.; Wu, L.; Zhu, Y.; Varanasi, K. K.; Gleason, K. K. Low-dimensional conduction mechanisms in highly conductive and transparent conjugated polymers. *Adv. Mater.* **2015**, *27*, 4604−4610.

(3) Sirringhaus, H.; Kawase, T.; Friend, R. H.; Shimoda, T.; Inbasekaran, M.; Wu, W.; Woo, E. P. High-resolution inkjet printing of all-polymer transistor circuits. *Science* **2000**, *290*, 2123−2126.

(4) Hebner, T. R.; Wu, C. C.; Marcy, D.; Lu, M. H.; Sturm, J. C. Ink-jet printing of doped polymers for organic light emitting devices. *Appl. Phys. Lett.* **1998**, *72*, 519−521.

(5) Shimoda, T.; Morii, K.; Seki, S.; Kiguchi, H. Inkjet printing of light-emitting polymer displays. *MRS Bull.* **2003**, *28*, 821−827.

(6) Shaheen, S. E.; Brabec, C. J.; Sariciftci, N. S.; Padinger, F.; Fromherz, T.; Hummelen, J. C. 2.5% efficient organic plastic solar cells. *Appl. Phys. Lett.* **2001**, *78*, 841−843.

(7) Peumans, P.; Uchida, S.; Forrest, S. R. *Materials for Sustainable Energy: A Collection of Peer-Reviewed Research and Review Articles from Nature Publishing Group*; World Scientific, 2011; pp 94−98.
(8) Granström, M.; Petritsch, K.; Arias, A. C.; Lux, A.; Andersson, M. R.; Friend, R. H. Laminated fabrication of polymeric photovoltaic diodes. *Nature* **1998**, *395*, 257−260.
(9) Peumans, P.; Forrest, S. R. Very-high-efficiency double-heterostructure copper phthalocyanine/C60 photovoltaic cells. *Appl. Phys. Lett.* **2001**, *79*, 126−128.
(10) Gundlach, D. J.; Lin, Y. Y.; Jackson, T. N.; Nelson, S. F.; Schlom, D. G. Pentacene organic thin-film transistors-molecular ordering and mobility. *IEEE Electron Device Lett.* **1997**, *18*, 87−89.
(11) Shtein, M.; Mapel, J.; Benziger, J. B.; Forrest, S. R. Effects of film morphology and gate dielectric surface preparation on the electrical characteristics of organic-vapor-phase-deposited pentacene thin-film transistors. *Appl. Phys. Lett.* **2002**, *81*, 268−270.
(12) Drury, C. J.; Mutsaers, C. M. J.; Hart, C. M.; Matters, M.; De Leeuw, D. M. Low-cost all-polymer integrated circuits. *Appl. Phys. Lett.* **1998**, *73*, 108−110.
(13) Stutzmann, N.; Friend, R. H.; Sirringhaus, H. Self-aligned, vertical-channel, polymer field-effect transistors. *Science* **2003**, *299*, 1881−1884.
(14) Burroughes, J. H.; Bradley, D. D. C.; Brown, A. R.; Marks, R. N.; Mackay, K.; Friend, R. H.; Burns, P. L.; Holmes, A. B. Light-emitting diodes based on conjugated polymers. *nature* **1990**, *347*, 539−541.
(15) Lee, C.-L.; Lee, K. B.; Kim, J.-J. Polymer phosphorescent light-emitting devices doped with tris(2-phenylpyridine) iridium as a triplet emitter. *Appl. Phys. Lett.* **2000**, *77*, 2280−2282.
(16) Braun, D.; Heeger, A. J. Visible light emission from semiconducting polymer diodes. *Appl. Phys. Lett.* **1991**, *58*, 1982−1984.
(17) Takeda, Y.; Hayasaka, K.; Shiwaku, R.; Yokosawa, K.; Shiba, T.; Mamada, M.; Kumaki, D.; Fukuda, K.; Tokito, S. Fabrication of ultra-thin printed organic TFT CMOS logic circuits optimized for low-voltage wearable sensor applications. *Sci. Rep.* **2016**, *6*, 25714.
(18) Koo, J. H.; Jeong, S.; Shim, H. J.; Son, D.; Kim, J.; Kim, D. C.; Choi, S.; Hong, J.-I.; Kim, D.-H. Wearable electrocardiogram monitor using carbon nanotube electronics and color-tunable organic light-emitting diodes. *ACS Nano* **2017**, *11*, 10032−10041.
(19) Meier, H.; Stalmach, U.; Kolshorn, H. Effective conjugation length and UV/vis spectra of oligomers. *Acta Polym.* **1997**, *48*, 379−384.
(20) Klaerner, G.; Miller, R. D. Polyfluorene derivatives: effective conjugation lengths from well-defined oligomers. *Macromolecules* **1998**, *31*, 2007−2009.
(21) Winokur, M. J.; Chunwachirasiri, W. Nanoscale structure-property relationships in conjugated polymers: Implications for present and future device applications. *J. Polym. Sci., Part B: Polym. Phys.* **2003**, *41*, 2630−2648.
(22) Troisi, A.; Shaw, A. Very Large π-Conjugation Despite Strong Nonplanarity: A Path for Designing New Semiconducting Polymers. *J. Phys. Chem. Lett.* **2016**, *7*, 4689−4694.
(23) Schwartz, B. J. CONJUGATEDPOLYMERS ASMOLECULARMATERIALS: How Chain Conformation and Film Morphology Influence Energy Transfer and Interchain Interactions. *Annu. Rev. Phys. Chem.* **2003**, *54*, 141−172.
(24) Vehoff, T.; Baumeier, B.; Troisi, A.; Andrienko, D. Charge Transport in Organic Crystals: Role of Disorder and Topological Connectivity. *J. Am. Chem. Soc.* **2010**, *132*, 11702−11708.
(25) Gagorik, A. G.; Savoie, B.; Jackson, N.; Agrawal, A.; Choudhary, A.; Ratner, M. A.; Schatz, G. C.; Kohlstedt, K. L. Improved Scaling of Molecular Network Calculations: The Emergence of Molecular Domains. *J. Phys. Chem. Lett.* **2017**, *8*, 415−421.
(26) Rivnay, J.; Mannsfeld, S. C. B.; Miller, C. E.; Salleo, A.; Toney, M. F. Quantitative Determination of Organic Semiconductor Microstructure from the Molecular to Device Scale. *Chem. Rev.* **2012**, *112*, 5488−5519.
(27) Noriega, R.; Rivnay, J.; Vandewal, K.; Koch, F. P. V.; Stingelin, N.; Smith, P.; Toney, M. F.; Salleo, A. A general relationship between disorder, aggregation and charge transport in conjugated polymers. *Nat. Mater.* **2013**, *12*, 1038−1044.
(28) Gu, K.; Snyder, C. R.; Onorato, J.; Luscombe, C. K.; Bosse, A. W.; Loo, Y.-L. Assessing the Huang-Brown Description of Tie Chains for Charge Transport in Conjugated Polymers. *ACS Macro Lett.* **2018**, *7*, 1333−1338.
(29) Yao, H.; Ye, L.; Zhang, H.; Li, S.; Zhang, S.; Hou, J. Molecular design of benzodithiophene-based organic photovoltaic materials. *Chem. Rev.* **2016**, *116*, 7397−7457.
(30) Jackson, N. E.; Savoie, B. M.; Marks, T. J.; Chen, L. X.; Ratner, M. A. The Next Breakthrough for Organic Photovoltaics? *J. Phys. Chem. Lett.* **2015**, *6*, 77−84.
(31) Mei, J.; Bao, Z. Side chain engineering in solution-processable conjugated polymers. *Chem. Mater.* **2014**, *26*, 604−615.
(32) Fauvell, T. J.; Zheng, T.; Jackson, N. E.; Ratner, M. A.; Yu, L.; Chen, L. X. Photophysical and morphological implications of single-strand conjugated polymer folding in solution. *Chem. Mater.* **2016**, *28*, 2814−2822.
(33) Panzer, F.; Bässler, H.; Köhler, A. Temperature Induced Order-Disorder Transition in Solutions of Conjugated Polymers Probed by Optical Spectroscopy. *J. Phys. Chem. Lett.* **2017**, *8*, 114−125.
(34) Scharsich, C.; Lohwasser, R. H.; Sommer, M.; Asawapirom, U.; Scherf, U.; Thelakkat, M.; Neher, D.; Köhler, A. Control of aggregate formation in poly(3-hexylthiophene) by solvent, molecular weight, and synthetic method. *J. Polym. Sci., Part B: Polym. Phys.* **2012**, *50*, 442−453.
(35) Liu, Y.; Zhao, J.; Li, Z.; Mu, C.; Ma, W.; Hu, H.; Jiang, K.; Lin, H.; Ade, H.; Yan, H. Aggregation and morphology control enables multiple cases of high-efficiency polymer solar cells. *Nat. Commun.* **2014**, *5*, 5293.
(36) Li, M.; Bin, H.; Jiao, X.; Wienk, M. M.; Yan, H.; Janssen, R. A. J. Controlling the Microstructure of Conjugated Polymers in High-Mobility Monolayer Transistors via the Dissolution Temperature. *Angew. Chem., Int. Ed.* **2020**, *59*, 846−852.
(37) Kline, R. J.; DeLongchamp, D. M.; Fischer, D. A.; Lin, E. K.; Richter, L. J.; Chabinyc, M. L.; Toney, M. F.; Heeney, M.; McCulloch, I. Critical Role of Side-Chain Attachment Density on the Order and Device Performance of Polythiophenes. *Macromolecules* **2007**, *40*, 7960−7965.
(38) Jackson, N. E. Coarse-Graining Organic Semiconductors: The Path to Multiscale Design. *J. Phys. Chem. B* **2021**, *125*, 485−496.
(39) Ricci, M.; Roscioni, O. M.; Querciagrossa, L.; Zannoni, C. MOLC. A reversible coarse grained approach using anisotropic beads for the modelling of organic functional materials. *Phys. Chem. Chem. Phys.* **2019**, *21*, 26195−26211.
(40) Gemünden, P.; Poelking, C.; Kremer, K.; Andrienko, D.; Daoulas, K. C. Nematic ordering, conjugation, and density of states of soluble polymeric semiconductors. *Macromolecules* **2013**, *46*, 5762−5774.
(41) Bowen, A. S.; Jackson, N. E.; Reid, D. R.; de Pablo, J. J. Structural correlations and percolation in twisted perylene diimides using a simple anisotropic coarse-grained model. *J. Chem. Theor. Comput.* **2018**, *14*, 6495−6504.
(42) Chiu, M.; Kee, T. W.; Huang, D. M. Coarse-Grained Simulations of the Effects of Chain Length, Solvent Quality, and Chemical Defects on the Solution-Phase Morphology of MEH-PPV Conjugated Polymers. *Aust. J. Chem.* **2012**, *65*, 463−471.
(43) Huang, D. M.; Faller, R.; Do, K.; Moulé, A. J. Coarse-Grained Computer Simulations of Polymer/Fullerene Bulk Heterojunctions for Organic Photovoltaic Applications. *J. Chem. Theory Comput.* **2010**, *6*, 526−537.
(44) Jankowski, E.; Marsh, H. S.; Jayaraman, A. Computationally Linking Molecular Features of Conjugated Polymers and Fullerene Derivatives to Bulk Heterojunction Morphology. *Macromolecules* **2013**, *46*, 5775−5785.
(45) Alessandri, R.; Uusitalo, J. J.; de Vries, A. H.; Havenith, R. W. A.; Marrink, S. J. Bulk Heterojunction Morphologies with Atomistic

https://doi.org/10.1021/acs.macromol.1c00302
Macromolecules 2021, 54, 3780−3789

Resolution from Coarse-Grain Solvent Evaporation Simulations. *J. Am. Chem. Soc.* **2017**, *139*, 3697−3705.
(46) Lee, C. K.; Hua, C. C.; Chen, S. A. An ellipsoid-chain model for conjugated polymer solutions. *J. Chem. Phys.* **2012**, *136*, 084901.
(47) Lee, C.-K.; Pao, C.-W. Multiscale Molecular Simulation of Solution Processing of SMDPPEH: PCBM Small-Molecule Organic Solar Cells. *ACS Appl. Mater. Interfaces* **2016**, *8*, 20691−20700.
(48) Marsh, H. S.; Jankowski, E.; Jayaraman, A. Controlling the Morphology of Model Conjugated Thiophene Oligomers through Alkyl Side Chain Length, Placement, and Interactions. *Macromolecules* **2014**, *47*, 2736−2747.
(49) Wilson, M. R. Molecular dynamics simulations of flexible liquid crystal molecules using a Gay-Berne/Lennard-Jones model. *J. Chem. Phys.* **1997**, *107*, 8654−8663.
(50) Shie, S. C.; Lee, C. K.; Hua, C. C.; Chen, S. A. A Predictive Coarse-Grained Model for Semiflexible Polymers in Specific Solvents. *Macromol. Theory Simul.* **2010**, *19*, 179−189.
(51) Jackson, N. E.; Bowen, A. S.; Antony, L. W.; Webb, M. A.; Vishwanath, V.; de Pablo, J. J. Electronic structure at coarse-grained resolutions from supervised machine learning. *Sci. Adv.* **2019**, *5*, No. eaav1190.
(52) Jackson, N. E.; Bowen, A. S.; de Pablo, J. J. Efficient Multiscale Optoelectronic Prediction for Conjugated Polymers. *Macromolecules* **2020**, *53*, 482−490.
(53) Rudyak, V. Y.; Gavrilov, A. A.; Guseva, D. V.; Tung, S.-H.; Komarov, P. V. Accounting for π-π stacking interactions in the mesoscopic models of conjugated polymers. *Mol. Syst. Des. Eng.* **2020**, *5*, 1137−1146.
(54) Grest, G. S.; Kremer, K. Molecular dynamics simulation for polymers in the presence of a heat bath. *Phys. Rev. A: At., Mol., Opt. Phys.* **1986**, *33*, 3628−3631.
(55) Kremer, K.; Grest, G. S. Dynamics of entangled linear polymer melts: A molecular-dynamics simulation. *J. Chem. Phys.* **1990**, *92*, 5057−5086.
(56) Ilnytskyi, J.; Wilson, M. R. A domain decomposition molecular dynamics program for the simulation of flexible molecules with an arbitrary topology of Lennard-Jones and/or Gay-Berne sites. *Comput. Phys. Commun.* **2001**, *134*, 23−32.
(57) Berardi, R.; Fava, C.; Zannoni, C. A Gay-Berne potential for dissimilar biaxial particles. *Chem. Phys. Lett.* **1998**, *297*, 8−14.
(58) Everaers, R.; Ejtehadi, M. R. Interaction potentials for soft and hard ellipsoids. *Phys. Rev. E: Stat., Nonlinear, Soft Matter Phys.* **2003**, *67*, 041710.
(59) Plimpton, S. Fast Parallel Algorithms for Short-Range Molecular Dynamics. *J. Comput. Phys.* **1995**, *117*, 1−19.
(60) Rossi, G.; Chance, R. R.; Silbey, R. Conformational disorder in conjugated polymers. *J. Chem. Phys.* **1989**, *90*, 7594−7601.
(61) McCulloch, B.; Ho, V.; Hoarfrost, M.; Stanley, C.; Do, C.; Heller, W. T.; Segalman, R. A. Polymer Chain Shape of Poly(3-alkylthiophenes) in Solution Using Small-Angle Neutron Scattering. *Macromolecules* **2013**, *46*, 1899−1907.
(62) Facchetti, A. π-Conjugated Polymers for Organic Electronics and Photovoltaic Cell Applications†. *Chem. Mater.* **2011**, *23*, 733−758.
(63) Graessley, W. W.; Hayward, R. C.; Grest, G. S. Excluded-Volume Effects in Polymer Solutions. 2. Comparison of Experimental Results with Numerical Simulation Data. *Macromolecules* **1999**, *32*, 3510−3517.
(64) Wang, D.; Yuan, Y.; Mardiyati, Y.; Bubeck, C.; Koynov, K. From Single Chains to Aggregates, How Conjugated Polymers Behave in Dilute Solutions. *Macromolecules* **2013**, *46*, 6217−6224.
(65) Schwartz, B. J. Conjugated polymers as molecular materials: How chain conformation and film morphology influence energy transfer and interchain interactions. *Annu. Rev. Phys. Chem.* **2003**, *54*, 141−172.
(66) Kuei, B.; Gomez, E. D. Chain conformations and phase behavior of conjugated polymers. *Soft Matter* **2017**, *13*, 49−67.
(67) Jackson, N. E.; Savoie, B. M.; Kohlstedt, K. L.; Olvera de la Cruz, M.; Schatz, G. C.; Chen, L. X.; Ratner, M. A. Controlling conformations of conjugated polymers and small molecules: The role of nonbonding interactions. *J. Am. Chem. Soc.* **2013**, *135*, 10475−10483.
(68) Berardi, R.; Zannoni, C.; Lintuvuori, J. S.; Wilson, M. R. A soft-core Gay-Berne model for the simulation of liquid crystals by Hamiltonian replica exchange. *J. Chem. Phys.* **2009**, *131*, 174107.
(69) Rathore, N.; Chopra, M.; de Pablo, J. J. Optimal allocation of replicas in parallel tempering simulations. *J. Chem. Phys.* **2005**, *122*, 024111.
(70) Nguyen, T.-Q.; Doan, V.; Schwartz, B. J. Conjugated polymer aggregates in solution: Control of interchain interactions. *J. Chem. Phys.* **1999**, *110*, 4068−4078.
(71) Yao, Z. F.; Wang, Z. Y.; Wu, H. T.; Lu, Y.; Li, Q. Y.; Zou, L.; Wang, J. Y.; Pei, J. Ordered Solid-State Microstructures of Conjugated Polymers Arising from Solution-State Aggregation. *Angew. Chem., Int. Ed.* **2020**, *59*, 17467−17471.
(72) Gennes, P. *The Physics of Liquid Crystals*; Clarendon Press: Oxford, 1974.
(73) Noguchi, H.; Saito, S.; Kidoaki, S.; Yoshikawa, K. Self-organized nanostructures constructed with a single polymer chain. *Chem. Phys. Lett.* **1996**, *261*, 527−533.
(74) Ivanov, V. A.; Paul, W.; Binder, K. Finite chain length effects on the coil-globule transition of stiff-chain macromolecules: A Monte Carlo simulation. *J. Chem. Phys.* **1998**, *109*, 5659−5669.
(75) Hu, D.; Yu, J.; Wong, K.; Bagchi, B.; Rossky, P. J.; Barbara, P. F. Collapse of stiff conjugated polymers with chemical defects into ordered, cylindrical conformations. *Nature* **2000**, *405*, 1030−1033.
(76) Schnurr, B.; Gittes, F.; MacKintosh, F. C. Metastable intermediates in the condensation of semiflexible polymers. *Phys. Rev. E: Stat., Nonlinear, Soft Matter Phys.* **2002**, *65*, 061904.
(77) Ivanov, V. A.; Stukan, M. R.; Müller, M.; Paul, W.; Binder, K. Phase diagram of solutions of stiff-chain macromolecules: A Monte Carlo simulation. *J. Chem. Phys.* **2003**, *118*, 10333−10342.
(78) Martemyanova, J. A.; Stukan, M. R.; Ivanov, V. A.; Müller, M.; Paul, W.; Binder, K. Dense orientationally ordered states of a single semiflexible macromolecule: An expanded ensemble Monte Carlo simulation. *J. Chem. Phys.* **2005**, *122*, 174907.
(79) Huang, W.; Huang, M.; Lei, Q.; Larson, R. A Simple Analytical Model for Predicting the Collapsed State of Self-Attractive Semiflexible Polymers. *Polymers* **2016**, *8*, 264.
(80) Lebold, K. M.; Noid, W. G. Dual approach for effective potentials that accurately model structure and energetics. *J. Chem. Phys.* **2019**, *150*, 234107.
(81) Chaimovich, A.; Shell, M. S. Coarse-graining errors and numerical optimization using a relative entropy framework. *J. Chem. Phys.* **2011**, *134*, 094112.
(82) Moore, T. C.; Iacovella, C. R.; McCabe, C. Derivation of coarse-grained potentials via multistate iterative Boltzmann inversion. *J. Chem. Phys.* **2014**, *140*, 224104.

https://doi.org/10.1021/acs.macromol.1c00302
Macromolecules 2021, 54, 3780−3789